Environment International 132 (2019) 105094

Contents lists available at ScienceDirect

Environment International

journal homepage: www.elsevier.com/locate/envint

Potential of PM-selected components to induce oxidative stress and root system alteration in a plant model organism

Diego Piacentini[a], Giuseppina Falasca[a], Silvia Canepari[b], Lorenzo Massimi[b,*]

[a] Department of Environmental Biology, Sapienza University of Rome, P. le Aldo Moro, 5, Rome 00185, Italy
[b] Department of Chemistry, Sapienza University of Rome, P. le Aldo Moro, 5, Rome 00185, Italy

ARTICLE INFO

Handling Editor: Da Chen

Keywords:
Arabidopsis thaliana
Atmospheric dust
Element bioaccumulation
Oxidative potential
Oxidative stress
Root morphology

ABSTRACT

Over the last years, various acellular assays have been used for the evaluation of the oxidative potential (OP) of particular matter (PM) to predict PM capacity to generate reactive oxygen (ROS) and nitrogen (RNS) species in biological systems. However, relationships among OP and PM toxicological effects on living organisms are still largely unknown. This study aims to assess the effects of atmospheric PM-selected components (brake dust - BD, pellet ash - PA, road dust - RD, certified urban dust NIST1648a - NIST, soil dust - S, coke dust - C and Saharan dust - SD) on the model plant *A. thaliana* development, with emphasis on their capacity to induce oxidative stress and root morphology alteration. Before growing *A. thaliana* in the presence of the PM-selected components, each atmospheric dust has been chemically characterized and tested for the OP through dithiothreitol (DTT), ascorbic acid (AA) and 2′,7′-dichlorofluorescin (DCFH) assays. After the exposure, element bioaccumulation in the *A. thaliana* seedlings, *i.e.*, in roots and shoots, was determined and both morphological and oxidative stress analyses were performed in roots. The results indicated that, except for SD and S, all the tested dusts affected *A. thaliana* root system morphology, with the strongest effects in the presence of the highest OPs dusts (BD, PA and NIST). Principal component analysis (PCA) revealed correlations among OPs of the dusts, element bioaccumulation and root morphology alteration, identifying the most responsible dust-associated elements affecting the plant. Lastly, histochemical analyses of NO and $O_2^{\cdot -}$ content and distribution confirmed that BD, PA and NIST induce oxidative stress in *A. thaliana*, reflecting the high OPs of these dusts and ultimately leading to cell membrane lipid peroxidation.

1. Introduction

Over the last few decades, particulate matter (PM) toxicity on living systems has been extensively evaluated by *in vitro* human cells culture and the generation of oxidative stress has been identified as one of the major mechanisms by which atmospheric particulate exerts its adverse biological effects (Evans et al., 2013; Cachon et al., 2014; Li et al., 2015). Oxidative stress is a general response of living organisms to many harmful environmental factors and it occurs when there is an imbalance between the level of reactive oxygen (ROS) and nitrogen (RNS) species and the natural antioxidant defence. High levels of ROS and RNS can cause lipid and protein oxidation, damages to nucleic acids, enzyme inhibition and activation of programmed cell death pathway (PCD), ultimately leading to cell death (Sharma et al., 2012).

During the last years, various experimental studies have provided a plausible correlation among PM toxicity and PM potential to generate ROS and RNS in biological systems (Shi et al., 2003a, 2003b; Nel, 2005; Brook et al., 2010; Kelly and Fussell, 2012). Acellular assays, such as dithiothreitol (DTT), ascorbic acid (AA) and 2′,7′-dichlorofluorescin (DCFH) assays, have been widely used to measure the oxidative potential (OP) of atmospheric particulate in order to provide a predictive index of the oxidative capacity of PM samples (Simonetti et al., 2018a).

In a recent study, Simonetti and co-authors (2018a) applied the DTT, AA and DCFH assays to the soluble and insoluble fractions of NIST1648a (urban dust certified for its elemental content; NIST) and other six types of widespread atmospheric dusts (brake dust, pellet ash, road dust, soil dust, coke dust and Saharan dust) characterized by very different chemical compositions, which can be associated with different

Abbreviations: AA, ascorbic acid; BD, brake dust; C, coke dust; DCFH, 2′,7′-dichlorofluorescin; DTT, dithiothreitol; LR, lateral root; LRD, lateral root density; LRP, lateral root primordium; NBT, nitro blue tetrazolium; NIST, certified urban dust NIST1648a; NO, nitric oxide; $O_2^{\cdot -}$, superoxide anion; OP, oxidative potential; PA, pellet ash; PCA, principal component analysis; PCD, programmed cell death; PM, particular matter; PR, primary root; PRL, primary root length; RD, road dust; RNS, reactive nitrogen species; ROS, reactive oxygen species; S, soil dust; SD, Saharan dust

* Corresponding author.
E-mail address: l.massimi@uniroma1.it (L. Massimi).

https://doi.org/10.1016/j.envint.2019.105094
Received 17 June 2019; Received in revised form 6 August 2019; Accepted 10 August 2019

adverse health effects (Marcoccia et al., 2017 and references therein). Brake dust (BD), produced by brake pads lining, contains high concentrations of heavy metals and toxic elements (Thorpe and Harrison, 2008; Canepari et al., 2010a). Pellet ash (PA) is a PM component, whose contribution increased during the last decades due to the diffusion of wood and pellet stoves for domestic heating (Reche et al., 2012). Road dust (RD) is a complex mixture of particles produced by mechanical abrasion of vehicle components (brakes, tires) and natural soil particles resuspended by vehicular traffic (Canepari et al., 2008; Pant and Harrison, 2013). Soil dust (S) is the major natural component of PM; Saharan dust (SD) constitutes a major contribute to PM during long-range transport (Perrino et al., 2016). Coke dust (C), produced by refinery plants, contains high concentrations of organic toxic species, which have been considered responsible for genotoxic and oxidative stress effects in animals and a risk for human health (Taioli et al., 2007; Vernile et al., 2013).

The three oxidative potential assays have provided very different results for each dust, confirming that none of the examined methods can be *a-priori* considered as representative of ROS and RNS generation pathways in biological organisms. Until now, few studies have been addressed to the *in vivo* evaluation of PM effects on plants or animals (Trifuoggi et al., 2019). Daresta et al. (2015) shown a toxic effect of PM_{10}, collected on quartz filters, on the root and shoot growth of tomato (*Solanum lycopersicum* L.) plants, while Popek et al. (2018) demonstrated a deleterious effect of PM on the efficiency of the photosynthetic apparatus of seven different deciduous plant species. Finally, Verma and Singh (2006) observed changes in the photosynthetic pigments, protein contents, leaf area and foliar surface architecture of two selected plant species grown in a highly auto-exhaust polluted area.

However, relationships among OP and PM toxicological effects on living organisms are still largely unknown (Costabile et al., 2019).

In this study, we assessed the OPs of the 7 PM-selected components (BD, PA, RD, NIST, S, C and SD) through the AA, DTT, and DCFH assays (OP^{AA}, OP^{DTT} and OP^{DCFH}) and studied their effects on *Arabidopsis thaliana* (L.) Heynh seedlings. The bioaccumulation of PM elements in exposed plants and the capacity of each dust to induce oxidative stress in the roots were evaluated. This plant was chosen as model organism because of its ease of growing in *in vitro* conditions.

The roots are common and primary target organs of soil pollution (Zanella et al., 2016; Ronzan et al., 2018). *Arabidopsis thaliana* root system consists of primary root (PR) established during embryogenesis and post-embryonic lateral roots (LRs), whose morphology and development may be severely damaged by the presence of heavy metals and toxic elements (Feigl et al., 2014; Fattorini et al., 2017) in a dose-dependent manner and with the strongest effects in case of multiple contaminations (Sofo et al., 2013; Vitti et al., 2014; Fattorini et al., 2017). These pollutants may induce the production of high levels of ROS and RNS, such as superoxide anion ($O_2\cdot^-$) and nitric oxide (NO), which can cause oxidative damages and lead to root-elongation and meristem growth inhibition, as well as root biomass reduction, possibly resulting in plant death (Singh et al., 2007; Achary et al., 2008; Yuan and Huang, 2016). Unsaturated lipid peroxidation of biological membranes is one of the most evident symptoms of oxidative stress, leading to plasma membrane integrity alteration, perturbing the bilayer structure and modifying membrane properties (Wong-Ekkabut et al., 2007).

This work aims to find correlations among the OP of the seven types of dust and their different capacity to alter primary root length (PRL) and lateral root density (LRD) and to generate ROS and RNS (high levels of $O_2\cdot^-$ and NO) in the root system of *A thaliana*. In addition, the element concentrations of each dust accumulated in the plant tissues were determined with the aim to identify the role of the single PM components in the alteration of the root system. Moreover, the correlations among OPs of the dusts, element bioaccumulation and root morphology alteration were individuated by performing principal component analysis (PCA). Lastly, NO, $O_2\cdot^-$ and lipid peroxidation content and cell/tissue distribution were performed to verify the induction of oxidative stress in the *A. thaliana* root apparatus by the selected atmospheric dusts.

2. Materials and methods

2.1. Collection and chemical analyses of the atmospheric dusts

Brake dust was collected from the brake linings of three different cars. Ash produced by pellet burning was collected from the hood of a domestic pellet stove. Road dust was obtained by collecting the dust deposited on the road surface at several traffic sites in the city centre of Rome (Central Italy). Certified material NIST1648a (Urban particulate matter, NIST1648A, Sigma-Aldrich) was used as urban dust. Soil dust was collected from rural areas around the city of Rome, within a perimeter of 50 km. Coke dust was collected from the ground in proximity of a coal park, near a refinery plant. Finally, Saharan dust was collected in Algeria, in the North of Sahara Desert. More details about the collection of the dusts are reported by Canepari et al. (2010b) and by Marcoccia et al. (2017).

Each dust is a quite complex mixture of particles having different size and morphology; therefore, they were homogenized, sieved at 50 μm (Giuliani, Torino, Italy) and stored at −20 °C until use. Chemical analyses of the dusts were performed by adapting to bulk dust an analytical procedure allowing the determination of both macro-components and trace elements on PM filters, previously optimized and validated by Canepari et al., 2006a, 2006b). The method used for the chemical analyses of the seven dusts is in accordance with Marcoccia et al. (2017).

2.2. Oxidative potential assays on the PM-selected components

50 mg of each dust were weighed (Analytical Balance Gibertini Elettronica E505, sensitivity of 0.01 mg) and then suspended in 50 mL of Milli-Q water (produced by Arioso UP 900 Integrate Water Purification System); the obtained suspensions were then stirred for 20 min by mechanical agitation. Subsequently, the three OP assays (AA, DTT, and DCFH) were applied to the suspension of the seven dusts and the samples were filtered through a nitrocellulose filter (0.45 μm pore size, Merck Millipore Ltd., Billerica, MA, USA) just prior to each instrumental analysis. The followed DTT, AA and DCFH procedures are detailed in Simonetti et al. (2018a). For each sample, three replicates were performed.

2.3. A. thaliana exposure to the PM-selected components

Seeds of *Arabidopsis thaliana* (L.) Heynh ecotype Columbia (Col, wild type, WT), were stratified and sterilized according to Della Rovere et al. (2013). The seeds were sown on a medium containing half-strength basal salt mixture (Duchefa Biochemie B·V, Haarlem, The Netherlands), 1% sucrose and 0.7% agar, at pH 5.8 (Murashige and Skoog, 1962) (Control). The medium was supplemented with 1000 mg L^{-1} of BD (BD), 125 μg L^{-1}, 250 μg L^{-1}, 500 μg L^{-1} or 1000 μg L^{-1} of PA (PA), 1000 mg L^{-1} of RD (RD), 1000 mg L^{-1} of NIST (NIST), 1000 mg L^{-1} of S, 1000 mg L^{-1} of C (C) and with 1000 mg L^{-1} of SD (SD), separately. The concentrations of the dusts were selected on the base of our preliminary unpublished data.

The seeds were grown in phytatrays (Phytatray™ II, P5929 Sigma-Aldrich; $n = 8$ seeds each phytatray and $n = 5$ phytatrays each treatment) for 11 days at 22 ± 2 °C, 70% humidity, 16 h light/8 h dark conditions and at white light (intensity 100 μEm^{-2} s^{-1}). Milli-Q water (produced by Arioso UP 900 Integrate Water Purification System) was used for all culture media. In this work, we proposed *A. thaliana* as a model organism to study root system organization, development and oxidative stress in relation to PM pollutants, due to its small size, easy growth requirements and simple root structure. In addition, to date *A. thaliana* represents the most widely studied species for research in plant

responses to environmental stresses. (Van Norman and Benfey, 2009).

2.4. Morphological analyses of A. thaliana root apparatus

Primary root length (PRL) and lateral root density (LRD) were evaluated in 30 seedlings per treatment. PRL was measured under a LEICA MZ8 stereomicroscope (Leica Microsystems, Wetzlar, Germany) using the AxioVision software (Carl Zeiss, Release 4.7.2) from digital images captured by Zeiss AxioCam camera (Zeiss, Oberkochen, Germany). Lateral roots (LRs) and lateral root primordia (LRPs) were observed and counted under light microscope, the corresponding LRD was calculated by dividing the total number of LRs and LRPs by the PR length where they were formed and expressed as mean number cm^{-1} (± SE).

2.5. Elemental chemical analysis of A. thaliana tissues

Element bioaccumulation was evaluated in 4 groups of 5 seedlings per treatment. For each dust exposure, 20 seedlings were sampled in order to obtain 4 replicates per treatment, each one containing 5 seedlings exposed to the same dust. The 5 seedlings of each replicate were washed for three times with Milli-Q water and then oven (Inter Continental Equipment) dried at 55 °C for 48 h. Subsequently, the seedlings were weighed and transferred into graduated 2.5 mL polyethylene tubes (Artiglass s.r.l., Due Carrare, PD, Italy) with the addition of 200 µL of ultrapure concentrated HNO_3 (67%; Promochem, LGC Standards GmbH, Wesel, Germany) and 100 µL of H_2O_2 (30%; Promochem, LGC Standards GmbH, Wesel, Germany). Each sample was then subjected to acid digestion for 30 min at 100 °C in an open vessel heated in a water bath, according to previous studies (Di Dato et al., 2017; Astolfi et al., 2018). After the acid digestion, the solutions were diluted into a final volume of 5 mL with Milli-Q water and then filtered through a pre-cleaned syringe filter (cellulose nitrate membranes, 0.45 µm pore size; GVS Filter Technology, Indianapolis, IN, USA). Fifteen of the 30 seedlings per treatment, previously analysed for root morphology, were also individually mineralised by using 100 µL of HNO_3 and 50 µL of H_2O_2 and then diluted into a final volume of 2.5 mL with Milli-Q water and filtered through a pre-cleaned syringe filter. Three blank solutions, consisting of Milli-Q water and reagents, were treated together with each digested sample set to trace possible contributions of sample contaminants.

Concentration of 32 elements (Al, As, Bi, Ca, Cd, Ce, Co, Cr, Cs, Cu, Fe, K, La, Li, Mg, Mn, Mo, Na, Nb, Ni, Pb, Rb, Sb, Sn, Sr, Ti, Tl, U, V, W, Zn, Zr) in the *A. thaliana* tissues of each sample was determined by using a quadrupole inductively coupled plasma mass spectrometer (ICP-MS, model 820-MS; Bruker, Bremen, Germany) equipped with a glass nebulizer (0.4 mL min^{-1}; Analytik Jena AG, Jena, Germany). For each element, external standard calibration curve was performed in the 1–500 µg L^{-1} range by serially diluting standard stock solutions (1000 ± 2 mg L^{-1}; Exaxol Italia Chemical Manufacturers Srl, Genoa, Italy; Ultra Scientific, North Kingstown, RI, USA; Merck Millipore Ltd., Billerica, MA, USA). Rhodium (1000 ± 2 mg L^{-1}; Panreac Química, Barcelona, Spain) was set at 5 µg L^{-1} as internal standard for all the measurements to control the nebulizer efficiency. Further details about the performance of the method and the used instrumental conditions are reported in Canepari et al. (2009) and in Astolfi et al. (2018), respectively.

Finally, the element concentrations were divided by the dry weight of each sample to obtain the element bioaccumulation expressed in µg g^{-1}.

Standard deviations of the four replicates per treatment were all below 20%.

2.6. Multivariate statistical analyses

Principal component analysis (Conti et al., 2007; Massimi et al., 2017, 2018), was performed to individuate correlations among the OPs of the dusts, element bioaccumulation and root morphology alteration in the plant model organism.

Multivariate statistical computations were operated on the data of the 15 seedlings per treatment morphologically and chemically analysed. The matrix of the data, composed of 119 samples (15 seedlings for each of the 7 treatments and 2 seedlings for each of the 7 controls) and 37 variables (3 dust OPs: OP^{AA}, OP^{DTT} and OP^{DCFH}; 32 element concentrations: Al, As, Bi, Ca, Cd, Ce, Co, Cr, Cs, Cu, Fe, K, La, Li, Mg, Mn, Mo, Na, Nb, Ni, Pb, Rb, Sb, Sn, Sr, Ti, Tl, U, V, W, Zn, Zr; 2 morphological measurements: PRL and LRD), was transformed by performing column mean centring and row and column autoscaling (to correct variations of the data due to the different scaling and units of the examined variables) and analysed by using the PCA. Multivariate statistical analyses were performed using the statistical software R (R-project for statistical computing, Ver. 3.0, 32-bit).

2.7. Detection of NO and $O_2\cdot^-$ accumulation in the A. thaliana root apparatus

Intracellular NO content in roots was quantified using the cell-permeable diacetate derivative diamino-fluorescein-FM (DAF-FM DA solution, D2321 Sigma-Aldrich). Five roots per treatment were incubated in 20 mM HEPES/NaOH buffer (pH 7.4) ($C_8H_{18}N_2O_4S$ ≥ 99.5%; H4034 Sigma-Aldrich; NaOH ≥98%; 30,620 Honeywell Fluka™) supplemented with 10 µM DAF-FM DA for 30 min at 25 °C (Liu et al., 2017). After washing three times with the buffer to remove the excess of the fluorescent probe, roots were observed using a LEICA DMRB microscope (Leica Microsystems, Wetzlar, Germany) equipped with the specific set of filters (EX 450–490, DM 510, LP 515). No significant epifluorescence signal was detectable with the buffer alone. The images were acquired with a LEICA DC500 digital camera and analysed with the IM1000 image-analysis software (Leica Microsystems).

Nitro blue tetrazolium (NBT) is a chemical compound that is reduced by superoxide anion ($O_2\cdot^-$) forming a purple/blue precipitate called formazan, thus representing a useful assay to study the intracellular production of the superoxide anion. Five *A. thaliana* roots per treatment were stained for 30 min in a solution of 0.5 mg mL^{-1} nitro blue tetrazolium (NBT; Roche Diagnostics Corp., Gmbh, Germany) in 10 mM Tris-HCl (pH 7.40 ± 0.05; T-2663 Sigma-Aldrich). After having transferred the roots in distilled water to stop the reaction, they were kept in the chloral hydrate solution ($Cl_3CCH(OH)_2$ crystallized, ≥98.0%; 23,100 Sigma-Aldrich) and instantly observed with LEICA DMRB light microscope equipped with Nomarski optics.

2.8. Visualization of lipid peroxidation in the A. thaliana root apparatus

Aldehydes that originated from lipid hydroperoxides (LOOHs) in the roots were visualized with Schiff's reagent (109033 Merk Millipore) as described by Yamamoto et al. (2003). Five root tips per treatment were excised and stained with Schiff's reagent for 20 min, rinsed with a freshly prepared sulphite solution (0.5% [*w/v*] $K_2S_2O_5$ in 0.05 m HCl; $K_2S_2O_5$ ≥ 98%; P2522 Sigma-Aldrich; HCl 32 wt% in H_2O; W530574 Sigma-Aldrich), and then kept in the chloral hydrate solution (Weigel and Glazebrook, 2002). After, they were mounted on microscope slides and observed with Nomarski optics applied to a LEICA DMRB microscope, equipped with a LEICA DC 500 camera. The image analysis was performed using LEICA IM1000 Image Manager Software (LEICA).

Fig. 1 shows a block diagram of the conducted research in the work.

3. Results and discussion

3.1. Oxidative potentials of the PM-selected components

Fig. 2 shows that the application of the three OP assays (AA, DTT,

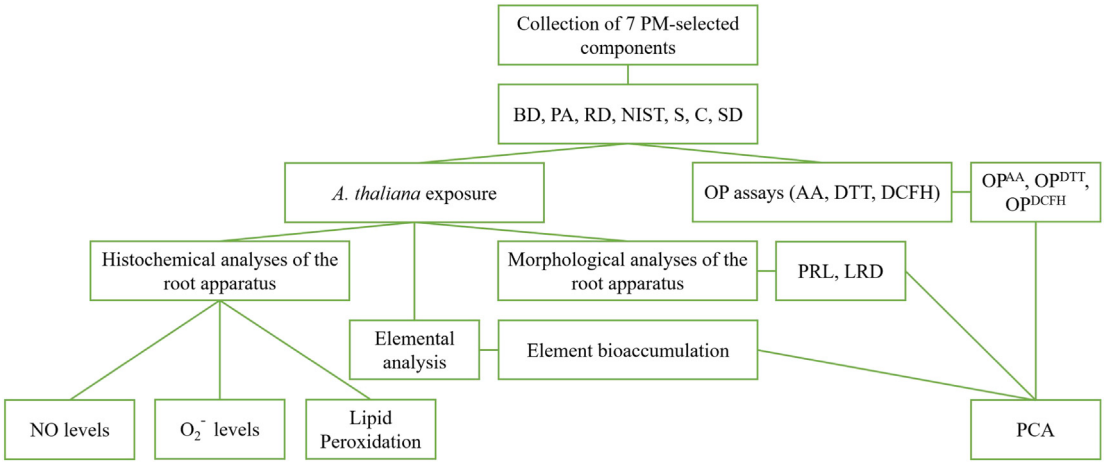

Fig. 1. Block diagram of the conducted research in the work.

and DCFH) to the seven atmospheric dusts gave different results. The AA assay was particularly sensitive toward BD and NIST, while DTT and DCFH assays were less selective and the highest OP^{DTT} and OP^{DCFH} values were obtained for PA (Fig. 2 A-C). In fact, chemical composition of dusts is a key factor in determining the redox behaviour of the samples (Perrone et al., 2016; Chirizzi et al., 2017).

The three OP assays have demonstrated to be responsive to different chemical compounds, thus showing a dissimilar response to atmospheric dusts coming from different sources (Bates et al., 2019). For example, AA has been usually found to be sensitive to metals like copper and iron, mainly released in coarse particles by mechanical abrasion of vehicle brakes (Simonetti et al., 2018b). On the other hand, DTT has been found to be responsive to copper as well as to several quinones (Charrier and Anastasio, 2012; Xiong et al., 2017) while both DTT and DCFH have demonstrated to be sensitive toward fine particles containing high amounts of organic compounds and mainly released by combustion processes such as biomass burning (Perrone et al., 2016).

Our results confirmed relevant differences in the relative sensitivity of the three assays toward the same dust. These results are in good agreement with those obtained by Simonetti et al. (2018a) for the insoluble fraction of the seven examined dusts. Overall, BD, PA and NIST were found to be the dusts with the highest oxidative potentials. These dusts are characterized by high concentrations of several dangerous compounds, such as heavy metals and toxic organic species (Marcoccia

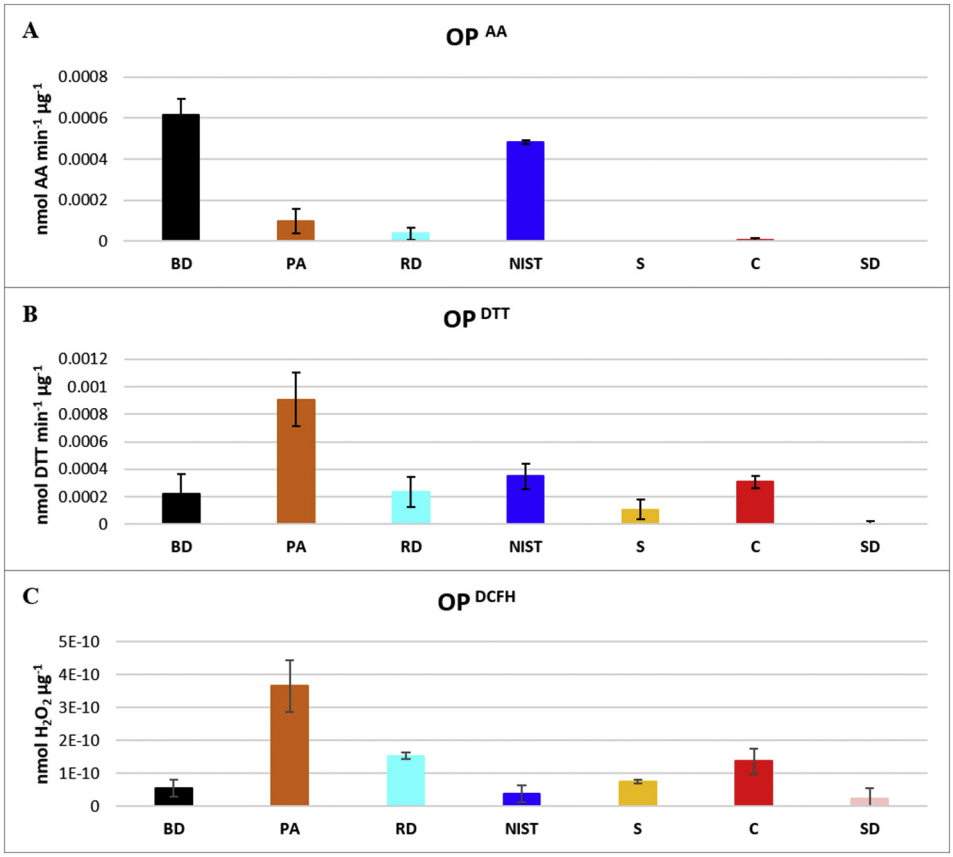

Fig. 2. Oxidative potentials of the 7 PM-selected components, obtained through ascorbic acid (AA, A), dithiothreitol (DTT, B) and 2′,7′-dichlorofluorescin (DCFH, C) assays. Means (± SE) of three technical replicates.

et al., 2017), which may be identified as the main responsible for the capacity of the dusts to generate oxidative stress. AA was confirmed to be particularly sensitive toward dusts released by resuspension of particles formed through the abrasion of vehicle brakes and tires, such as BD and NIST. The high OP^{DCFH} and OP^{DTT} of PA suggest that emission of particles containing high concentrations of secondary organics (such as oxygenated polycyclic aromatic hydrocarbons) from biomass pellet burning, may drives oxidative responses in biological organisms, thus being particularly harmful for human health (Gilardoni et al., 2016). It is worth noting that the role on the adverse health effects of biomass burning, whose contribution to PM is increasing in the last years, is a very interesting issue that still requires further explorations.

To our knowledge, previous studies have been mostly focused on the oxidative potential evaluation of the soluble fraction of PM samples, which is thought to be more indicative of the ability of the dusts to generate ROS and RNS in living organisms. However, since the *A. thaliana* seedlings were exposed to both the soluble and insoluble PM-selected components, it must be considered that also the insoluble particles contained in the atmospheric dusts may have direct contact with the cells of the *A. thaliana* root and so may establish *in vivo* redox equilibria. In fact, although the interactions of the insoluble particles with living organisms are still largely unknown, it is well known that PM released by combustion processes contains insoluble nanoparticles that are deemed to be able to enter organisms (Canepari et al., 2010a). This behaviour allows us to hypothesize a possible role of both the soluble and insoluble PM components in the generation of the oxidative stress (Knaapen et al., 2004; Zou et al., 2016).

3.2. Effects of the PM-selected components on the A. thaliana root growth and morphology

Morphology and development of PR and LR of *A. thaliana* seedlings grown in the presence of the dusts were differently altered. Fig. 3 shows that BD heavily and significantly ($P < 0.001$) inhibited PR growth (*i.e.*, 91,2%) and reduced lateral root density of 25% compared to Control. This behavior may be due to the high heavy metal and toxic element content in BD, as recently reported (Dodd et al., 2014; Maiorana et al., 2019).

Pellet ash treatment markedly affected PRL ($P < 0.01$), while no statistically significant effects were detected for LRD (Fig. 3). It is worth noting that in the case of PA, we tested several concentrations, but the dramatic effects of PA at concentrations higher than 125 μg L^{-1} on plant germination and development, did not allow us to measure PRL and LRD. Therefore, we reported the results obtained by using 125 μg L^{-1} (Fig. 3). PA-treated root growth inhibition may be related to the high concentrations of Mn, toxic elements and organic toxic substances such as polycyclic aromatic hydrocarbons, which are released from wood pellet stove for domestic heating (Toscano et al., 2014; Abdoli et al., 2018). Road dust treatment altered root development by reducing LRD of 30.8% in comparison with Control ($P < 0.01$, Fig. 3 B). This behavior may be related to the high As content in RD; in fact, it has been demonstrated that high As concentration can lead to alteration of *A. thaliana* root formation and development (Fattorini et al., 2017). Urban dust exposure did not significantly alter PRL, while negatively affected LRD, which was reduced by 59.3% in comparison with Control ($P < 0.001$, Fig. 3 B). Soil dust treatment increased PRL of 28.5% compared to Control ($P < 0.01$), while no significant effects were detected for LRD (Fig. 3). In the coke dust treatment, we observed an increase of PR growth ($P < 0.05$) and a reduction of LRD of 46.2%

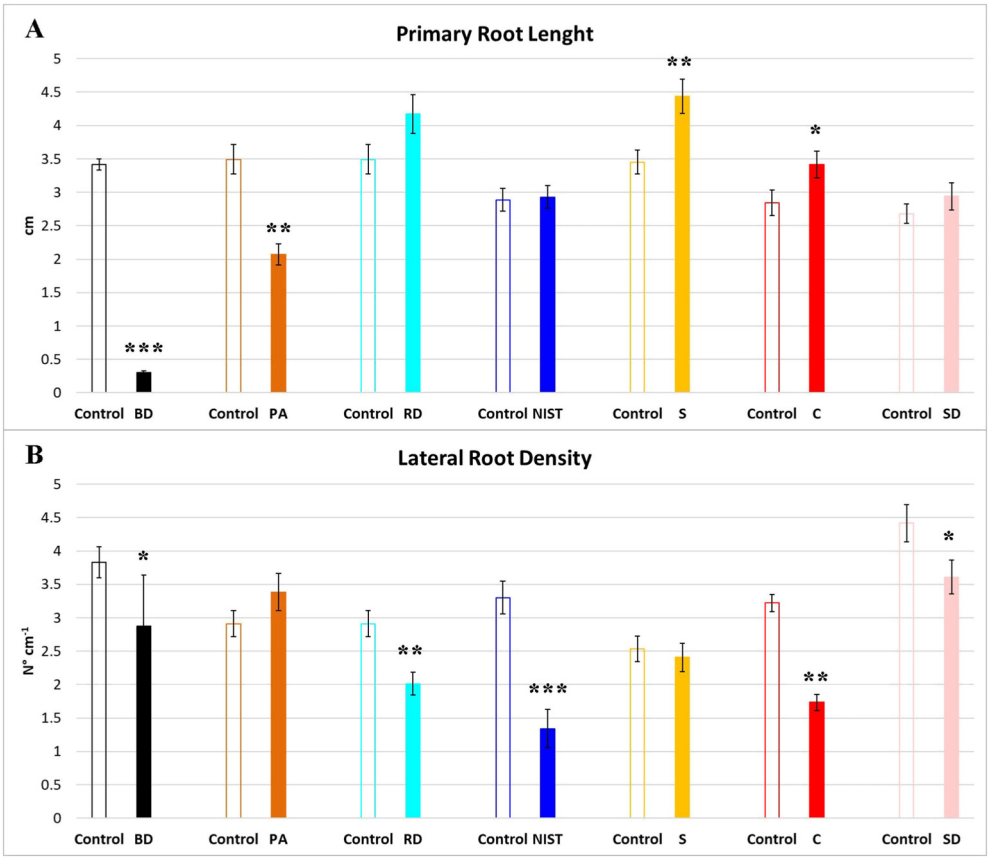

Fig. 3. Means (± SE) of primary root length and lateral root density of *A. thaliana* seedlings, exposed to the seven dusts. Asterisks represent statistical significance with respect to control at *$P < 0.05$, **$P < 0.01$ and ***$P < 0.001$ (Student's *t*-test).

Table 1
Accumulation of the elements of the seven dusts in the *A. thaliana* seedlings (μg g^{-1}).

Elements	Mean of all controls		BD		PA		RD		NIST		S		C		SD	
			1000 mg L^{-1}		125 mg L^{-1}		1000 mg L^{-1}		1000 mg L^{-1}		1000 mg L^{-1}		1000 mg L^{-1}		1000 mg L^{-1}	
	Mean	*SD*	**Mean**	*SD*	**Mean**	*SD*	**Mean**	*SD*	**Mean**	*SD*	**Mean**	*SD*	**Mean**	*SD*	**Mean**	*SD*
Al	**100**	*7*	**452**	*72*	**68**	*13*	**68**	*14*	**828**	*3*	**180**	*22*	**99**	*13*	**37**	*4*
As	**0.28**	*0.06*	**0.97**	*0.19*	**0.065**	*0.14*	**1.2**	*0.2*	**0.0011**	*0.0003*	**0.33**	*0.06*	**1.0**	*0.2*	**0.055**	*0.007*
Bi	**0.22**	*0.01*	**0.79**	*0.12*	**0.099**	*0.019*	**0.043**	*0.011*	**0.58**	*0.06*	**0.036**	*0.005*	**0.030**	*0.007*	**0.031**	*0.009*
Ca	**9226**	*798*	**28,176**	*1827*	**8731**	*1477*	**7621**	*1298*	**22,204**	*397*	**10,402**	*1748*	**10,035**	*1868*	**2449**	*378*
Cd	**1.0**	*0.2*	**0.72**	*0.03*	**0.29**	*0.04*	**0.11**	*0.03*	**7.5**	*0.5*	**0.31**	*0.04*	**0.81**	*0.09*	**0.68**	*0.05*
Ce	**1.1**	*0.2*	**2.1**	*0.2*	**0.20**	*0.05*	**0.24**	*0.06*	**2.5**	*0.6*	**0.72**	*0.18*	**0.38**	*0.06*	**1.3**	*0.2*
Co	**0.68**	*0.01*	**2.0**	*0.2*	**0.21**	*0.06*	**0.14**	*0.04*	**1.9**	*0.3*	**0.31**	*0.02*	**0.34**	*0.03*	**0.40**	*0.08*
Cr	**16**	*1*	**28**	*5*	**2.8**	*0.6*	**2.3**	*0.5*	**75**	*19*	**4.2**	*0.9*	**13**	*1*	**26**	*6*
Cs	**0.071**	*0.006*	**0.68**	*0.05*	**0.017**	*0.002*	**0.019**	*0.004*	**0.37**	*0.01*	**0.057**	*0.009*	**0.024**	*0.002*	**0.026**	*0.004*
Cu	**36**	*2*	**194**	*8*	**15**	*2*	**14**	*2*	**64**	*1*	**27**	*3*	**28**	*5*	**14**	*1*
Fe	**521**	*36*	**2389**	*53*	**262**	*34*	**259**	*31*	**2102**	*115*	**359**	*37*	**346**	*22*	**526**	*67*
K	**18,668**	*3004*	**19,529**	*1017*	**43,621**	*8114*	**27,226**	*4528*	**40,736**	*3067*	**4363**	*356*	**23,318**	*4530*	**12,106**	*916*
La	**0.54**	*0.06*	**0.20**	*0.03*	**0.092**	*0.012*	**0.12**	*0.02*	**1.4**	*0.2*	**0.49**	*0.02*	**0.26**	*0.03*	**0.80**	*0.20*
Li	**0.57**	*0.03*	**3.5**	*0.1*	**0.14**	*0.03*	**0.12**	*0.02*	**1.5**	*0.1*	**0.41**	*0.14*	**0.18**	*0.04*	**0.10**	*0.02*
Mg	**1690**	*49*	**2043**	*47*	**1661**	*244*	**1311**	*56*	**2946**	*265*	**1188**	*99*	**1463**	*284*	**1594**	*385*
Mn	**200**	*26*	**214**	*9*	**1388**	*361*	**180**	*31*	**332**	*31*	**168**	*31*	**320**	*30*	**216**	*45*
Mo	**7.3**	*0.8*	**6.0**	*0.1*	**11**	*2*	**11**	*2*	**10**	*1*	**4.7**	*1.5*	**11**	*1*	**4.4**	*0.6*
Na	**2671**	*342*	**10,352**	*732*	**2930**	*1570*	**2783**	*2154*	**6832**	*1166*	**2579**	*815*	**2496**	*672*	**2371**	*1695*
Nb	**0.079**	*0.004*	**0.56**	*0.12*	**0.0070**	*0.0020*	**0.0074**	*0.0034*	**0.23**	*0.05*	**0.017**	*0.004*	**0.018**	*0.003*	**0.016**	*0.002*
Ni	**20**	*1*	**40**	*1*	**4.4**	*0.8*	**4.7**	*1.0*	**102**	*16*	**6.3**	*0.6*	**10**	*1*	**31**	*9*
Pb	**4.0**	*0.2*	**29**	*2*	**0.8**	*0.1*	**1.0**	*0.2*	**37**	*1*	**6.6**	*0.5*	**6.1**	*1.0*	**2.79**	*0.82*
Rb	**6.3**	*1.2*	**11**	*1*	**7.8**	*1.3*	**5.0**	*1.1*	**16**	*2*	**2.6**	*0.6*	**5.0**	*1.1*	**6.2**	*1.2*
Sb	**0.38**	*0.03*	**9.7**	*0.4*	**0.18**	*0.03*	**0.11**	*0.02*	**1.7**	*0.1*	**0.20**	*0.05*	**0.15**	*0.04*	**0.086**	*0.019*
Sn	**0.49**	*0.09*	**3.6**	*0.2*	**0.21**	*0.05*	**3.8**	*0.8*	**3.2**	*0.4*	**0.31**	*0.04*	**0.26**	*0.06*	**0.22**	*0.04*
Sr	**21**	*1*	**19**	*3*	**20**	*4*	**31**	*5*	**40**	*5*	**68**	*11*	**57**	*5*	**31**	*5*
Ti	**4.6**	*0.1*	**11**	*1*	**2.5**	*0.4*	**2.3**	*0.3*	**28**	*1*	**5.4**	*1.0*	**4.6**	*0.8*	**3.3**	*0.3*
Tl	**0.058**	*0.002*	**0.69**	*0.13*	**0.035**	*0.007*	**0.010**	*0.002*	**0.12**	*0.02*	**0.059**	*0.011*	**0.031**	*0.003*	**0.013**	*0.002*
U	**0.076**	*0.002*	**0.25**	*0.07*	**0.0074**	*0.0014*	**0.012**	*0.003*	**0.13**	*0.01*	**0.061**	*0.007*	**0.027**	*0.001*	**0.026**	*0.003*
V	**0.34**	*0.02*	**3.9**	*0.2*	**0.24**	*0.08*	**0.23**	*0.06*	**3.7**	*0.1*	**1.5**	*0.3*	**5.5**	*0.4*	**0.32**	*0.05*
W	**0.035**	*0.007*	**0.98**	*0.04*	**0.28**	*0.05*	**0.017**	*0.003*	**0.25**	*0.01*	**0.077**	*0.011*	**0.074**	*0.018*	**0.040**	*0.007*
Zn	**409**	*36*	**1561**	*123*	**171**	*32*	**171**	*33*	**825**	*40*	**358**	*52*	**916**	*80*	**296**	*39*
Zr	**0.34**	*0.02*	**5.8**	*1.1*	**0.11**	*0.04*	**0.11**	*0.04*	**2.6**	*0.1*	**0.35**	*0.06*	**0.068**	*0.013*	**0.16**	*0.01*

($P < 0.01$). The high organic content in C (Marcoccia et al., 2017) may explain the negative effects of this treatment on *A. thaliana* root system.

Lastly, no strong effects on *A. thaliana* root morphology and development were detected for SD treatment. Saharan dust had slight and no significant effects on *A. thaliana* roots probably because of its low metallic content (Marcoccia et al., 2017) (Fig. 3).

In addition, the different responses between PRL and LRD to the same dust might be explained by considering the different origins of PRs and LRs; embryonically pre-formed the first, post-embryonically formed the latter.

3.3. Accumulation of the elements of the PM-selected components in the A. thaliana seedlings

Accumulation of the elements of the atmospheric dusts in the *A. thaliana* tissues after 11 days exposure to 1000 mg L^{-1} of BD, RD, NIST, S, C, SD and to 125 mg L^{-1} of PA, is reported in Table 1. Results of the elemental analyses showed that the most bioaccumulated elements were Cd, Ce, Co, Cu, Fe, Mn, Pb, Sb, Sn, Ti, V, Zn and Zr. As expected, element concentrations in the exposed individuals were extremely variable depending on the dust type, and, in most cases, considerably higher than the control. The enrichment factors (ratio between the concentration in exposed and in control individuals) were particularly high (up to about five times) for Cs, Li, Nb, Pb, Sb, Sn, Tl, V, W and Zr after exposure to BD; Mn and W after exposure to PA; Sn after exposure to RD; Al, Cd, Pb, Sn, Ti, V, W, Zr after exposure to NIST; and V after exposure to C. In general, the enrichment factors tended to increase together with the increase of the element concentration in the different dusts. In fact, Mn and Pb are the most concentrated elements in PA and NIST, respectively, while Cu, Sb and Sn are the main constituents of BD. On the other hand, high amounts of Sn are in RD, V is one of the most abundant elements in C, and heavy metals and toxic elements are less concentrated in S and SD (Marcoccia et al., 2017).

Pearson correlation coefficients among the element concentration in the dusts and in the *A. thaliana* tissues were calculated to verify the element bioaccumulation capacity of *A. thaliana*. Low bioaccumulation capacity was found for As, Bi, Ca, Cr, Cs, K, La, Li, Mg, Mo, Na, Nb, Ni, Rb, Sr, Tl, U and W (Person coefficients < 0.5), while Cd, Ce, Co, Cu, Fe, Mn, Pb, Sb, Sn, Ti, V, Zn and Zr were efficiently bioaccumulated (Person coefficients > 0.5). Among these elements, Cd, Co, Cu, Mn and Sb were found to be the most bioaccumulated (Person coefficients > 0.8).

Overall, *A. thaliana* turned out to be able to accumulate high amounts of elements released through the abrasion of vehicle brakes, such as Cu, Fe, Mn, Sb, Sn (Massimi et al., 2019), and tires, such as Zn (Councell et al., 2004), whose concentrations are particularly high in BD, RD and NIST. Besides, it was able to accumulate high amounts of Mn and Pb released in particles produced by biomass pellet burning (Simonetti et al., 2018b), whose concentrations are particularly high in PA.

3.4. Principal component analysis

Principal component analysis was performed to individuate correlations among OPs of the dusts, element bioaccumulation and root morphology alteration, in order to identify the most responsible dust-associated elements affecting the model plant growth. Five significant components accounting for 83.94% were obtained (the scores and loadings are shown in supplementary material S1); the variance explained by each component is: 47.58%, 18.32%, 10.12%, 4.48% and

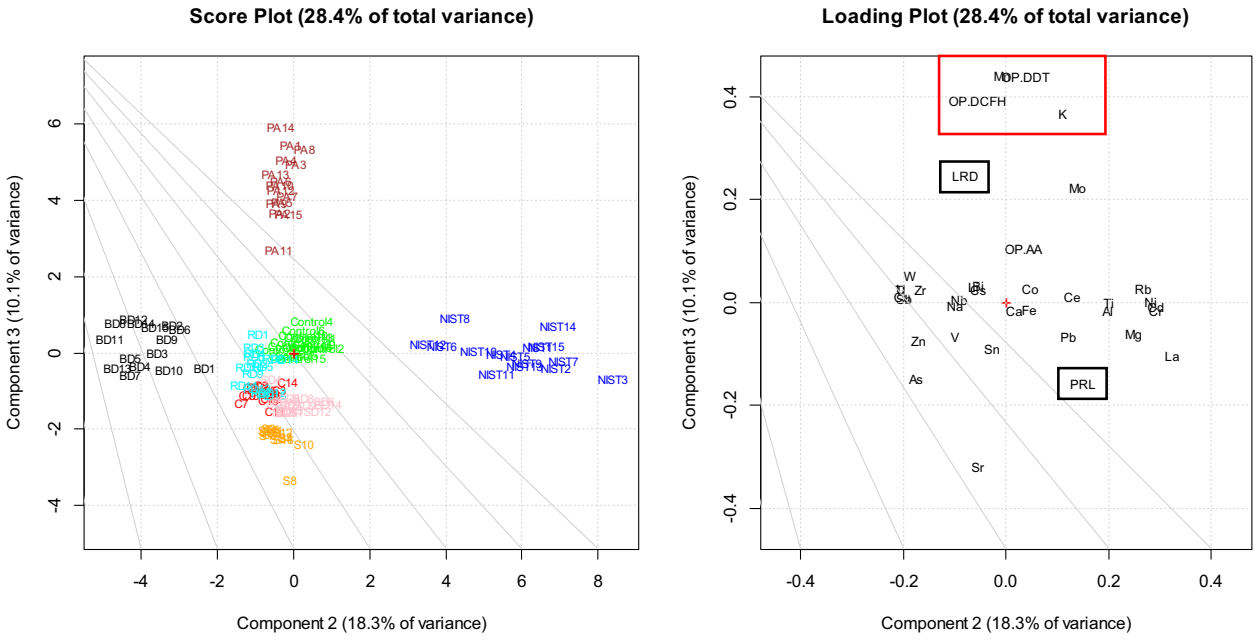

Fig. 4. Score plot and loading plot of PC2 and PC3 of the PCA performed on the OPs of the dusts, element bioaccumulation and PRL and LRD alteration in the *A. thaliana* seedlings.

3.44%.

First component (PC1), which explains the 47.58% of the total variance, well separates the samples whereby the highest concentrations of elements for which AA is particularly sensitive were bioaccumulated (*A. thaliana* seedlings exposed to BD and NIST) from the others. However, PC1, along with the second component (PC2), is unable to separate the samples exposed to PA, RD, C, SD and S from the controls (score plot and loading plot of PC1 and PC2 are shown in supplementary material S1). PC2 well explains the element bioaccumulation variability between the samples exposed to BD and the samples exposed to NIST while the third component (PC3) well separates the samples exposed to PA from the others depending on the Mo, Mn and K bioaccumulation and the OP^{DTT} and OP^{DCFH} variability in the PM-selected components. Therefore, PC2 and PC3, which explain the 28.42% of the total variance, were represented, since they better reflect the element bioaccumulation and OPs variability in all the examined samples. PCA results are summarized in the score plot and in the loading plot of Fig. 4.

From Fig. 4, we can observe that the samples are separated along PC2 and PC3 depending on the OP^{AA}, OP^{DTT} and OP^{DCFH} of the dusts, the element concentrations accumulated in the *A. thaliana* tissues, and the PRL and LRD of the examined seedlings after each dust exposure. The controls are plotted on the central part of the score plot, thus showing PRL and LRD mean values and no element bioaccumulation, since they were not grown in the presence of PM-selected components. BD samples are in the left part of the score plot, in the opposite direction along PC2 respect to PRL of the loading plot, since the seedlings exposed to brake dust showed the highest PRL reduction. From the loading plot, we can observe that in BD samples, the high bioaccumulation of As, Bi, Cs, Cu, Li, Na, Nb, Sb, Sn, Tl, U, V, W, Zn and Zr may be responsible for the strong inhibition of the primary root growth. On the other hand, NIST samples are plotted on the right part of the score plot, since the seedlings exposed to urban dust showed a slight increase of PRL and the highest decrease of LRD.

From the loading plot, we can observe that the inhibition of the lateral root production may be due to the high bioaccumulation of Al, Cd, Ce, Cr, La, Mg, Ni, Pb, Rb and Ti. In fact, as previously mentioned, it is well known that the root cell division and differentiation pattern may be severely damaged by the presence of heavy metals such as Cd, Cr, Ni and Pb, in a dose-dependent manner and with the strongest effects in case of multiple contamination (Vitti et al., 2014; Zanella et al., 2016; Fattorini et al., 2017). On the contrary, PA samples are in the upper part of the score plot, since the seedlings exposed to pellet ash showed a strong reduction of PRL ($P < 0.01$) and a slight and not statistically significance increase of LRD. From the loading plot, in PA samples the highest concentrations of K and Mn were bioaccumulated; these elements could be then responsible for the inhibition of the primary root length growth as reported by Zhao et al. (2017). Finally, RD, C, S and SD samples are plotted on the central lower part of the score plot, since the *A. thaliana* seedlings exposed to road dust, coke dust, soil dust and Saharan dust, showed a slight PRL increase and LRD reduction, which may be attributed to the high bioaccumulation of As, Sn, Sr, V and Zn. Arsenic and tin were mostly bioaccumulated in RD samples, strontium in S samples, and vanadium and zinc in C samples.

OPs of the dusts are all plotted on the upper part of the loading plot, in the same direction of PA samples. OP^{DTT} and OP^{DCFH} were found to be well correlated with the K and Mn concentrations accumulated in the *A. thaliana* seedlings exposed to PA, while OP^{AA} appeared to be related with Mo and other elements bioaccumulated in BD, RD and NIST samples (Bi, Ce, Co, Cs, Cu, Li, Mo, Nb, Ni, Rb, Sb, Ti, Tl, U, W and Zr). These results agree with those obtained in Simonetti et al. (2018a), where Mn concentration has been found to be highly correlated with the OP^{DTT} and the OP^{DCFH} of the insoluble fraction of PA and Co, Ce, Cu, Mo, Ni, Ti and Zr have been identified as responsible for the generation of the OPs of BD and NIST. Lastly, OP^{AA}, OP^{DTT} and OP^{DCFH} are plotted on the opposite direction respect to PRL; this indicates that OPs of the dusts are positively correlated with PRL reduction. Therefore, since primary root is established during the *A. thaliana* embryogenesis and the inhibition of the primary root length was observed only in BD, PA and NIST samples, we can suppose that brake dust, pellet ash and urban dust induced oxidative stress during the early stages of post-embryogenic development of the exposed seedlings. This led to a slight increase of the post-embryonic lateral root production only in the case of PA exposure. Overall, pellet ash, which contains toxic elements and toxic organic compounds was found to be the dust with the highest potential to induce oxidative stress in the test living organism (de Oliveira Alves et al., 2011).

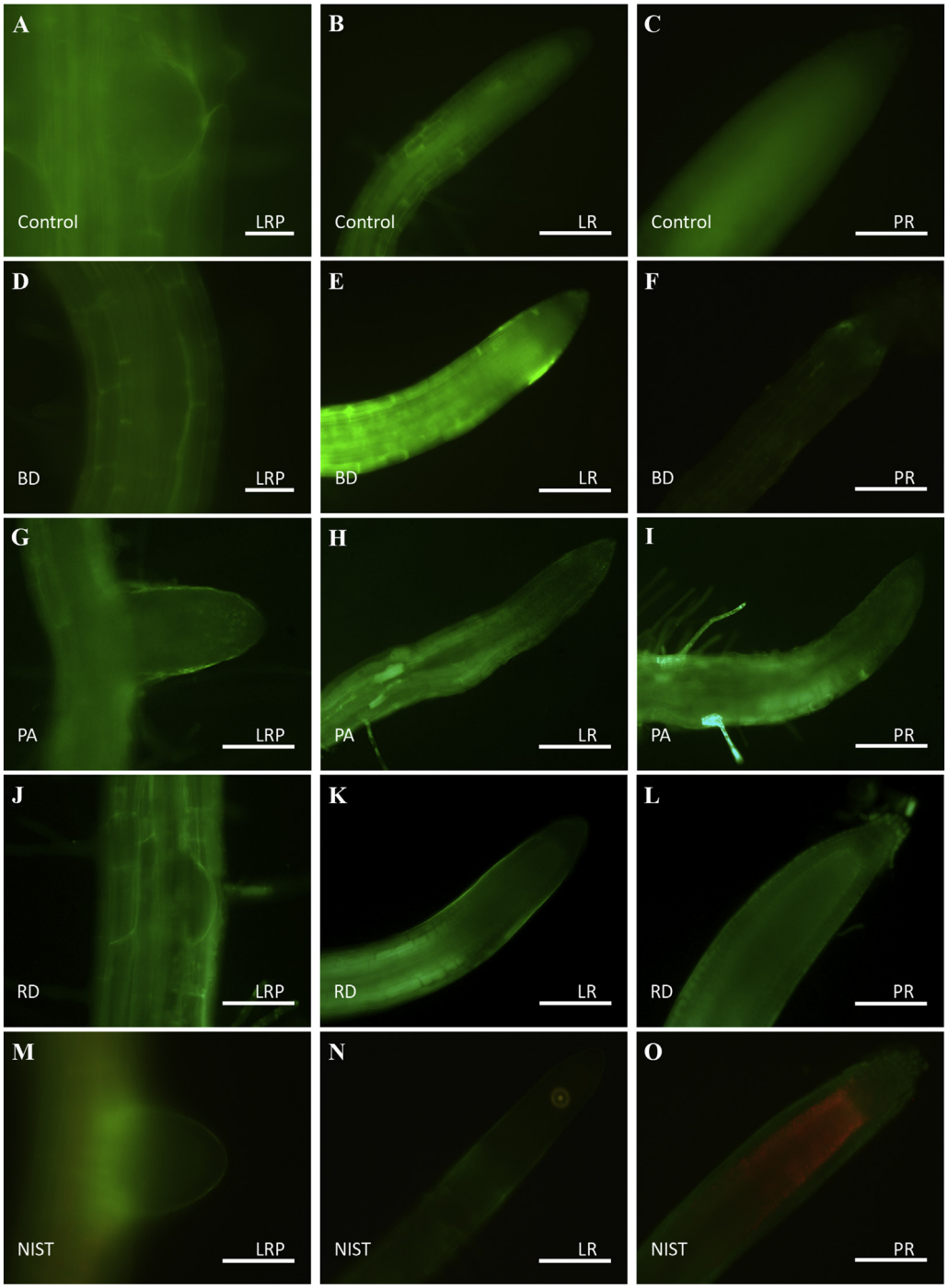

Fig. 5. NO signal (bright green color) in *A. thaliana* LRPs, LRs and PRs not exposed (control, A–C) or exposed to BD (D–F), PA (G–I), RD (J–L) and NIST (M–O). Bars = 30 μm (A, M) and 100 μm (B–L, N–O). (For interpretation of the references to color in this figure legend, the reader is referred to the web version of this article.)

3.5. Detection of NO and $O_2\cdot^-$ levels and lipid peroxidation in A. thaliana roots

The roots of 11-days old *A. thaliana* seedlings grown in the presence of BD, PA, RD and NIST were collected and treated for NO, $O_2\cdot^-$ and lipid peroxidation visualization, respectively, to verify if the PM-selected components may trigger to oxidative stress in the tested biological system. The endogenous level and distribution of NO in roots greatly changed with respect to the control depending on the type of atmospheric dust tested (Fig. 5).

In the roots grown in control conditions, NO expression was weak and mainly localized in the epidermis of LRPs and both in the vascular tissues and cortical parenchyma of LRs and PRs, while low NO expression was detected in the root apical meristem (Fig. 5, A-C).

Brake dust and PA deeply increased and delocalized endogenous NO in *A. thaliana* roots respect to the control (Fig. 5 D-I and A-C in comparison). Pellet ash increased NO production in all the tissues of both LRs and PRs and in the epidermis of LRPs as well, while BD strongly increased NO level and distribution in the stele, cortex and epidermis of the LRs. Road dust weak increased NO signal in the cortex and epidermis of LRs tip and mature zone (Fig. 5, J-L). Interestingly, NIST treated roots showed reduced level of NO both in LRs and PRs respect to

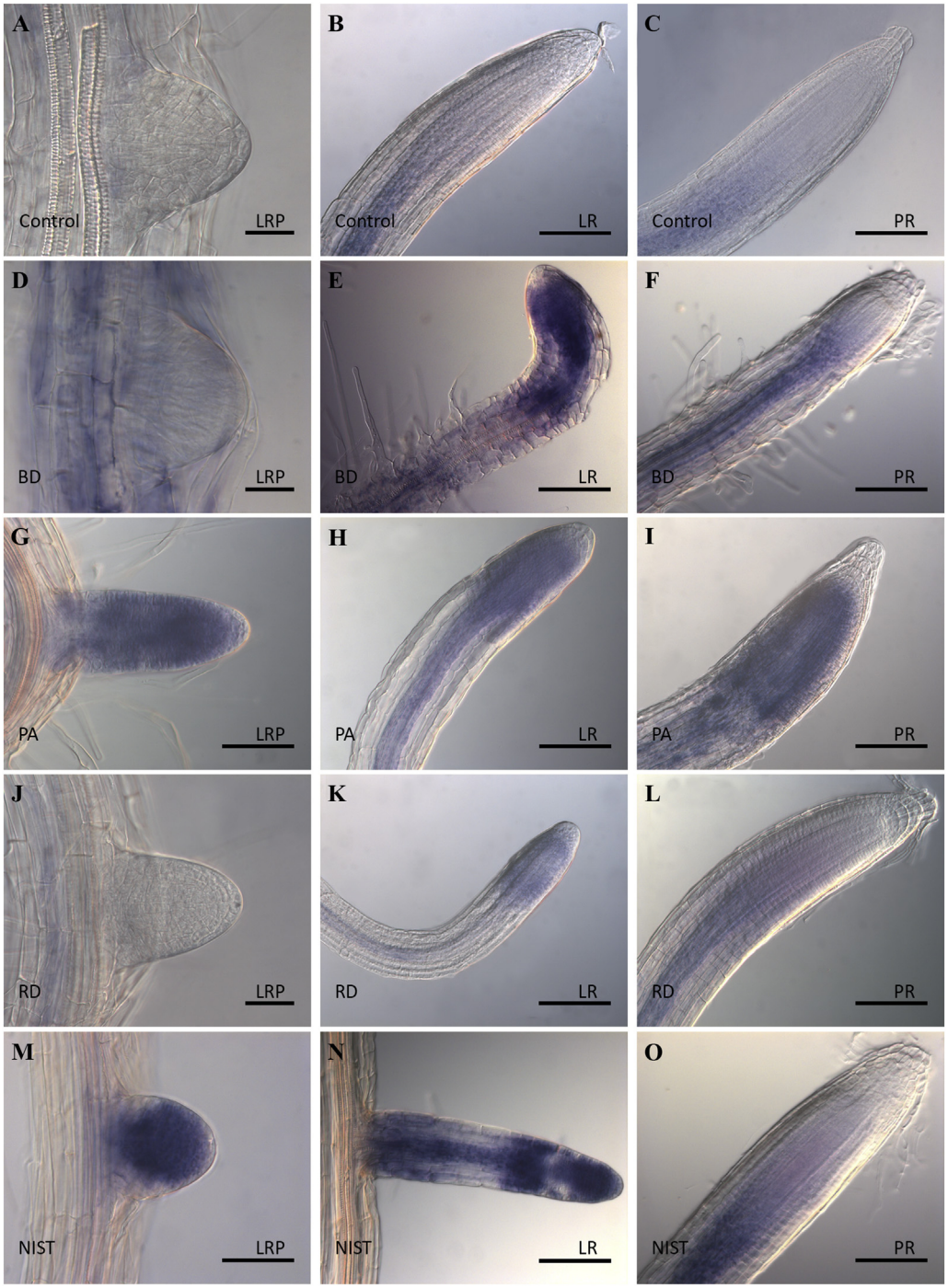

Fig. 6. Superoxide radical (purple/blue color) detected by NBT staining in *A. thaliana* LRPs, LRs and PRs not exposed (control, A–C) or exposed to BD (D–F), PA (G–I), RD (J–L) and NIST (M–O). Bars = 30 μm (A, D, M) and 100 μm (B–C; E–L; N–O). (For interpretation of the references to color in this figure legend, the reader is referred to the web version of this article.)

the control (Fig. 5, M-O). This result indicates that the endogenous level and distribution of NO in *A. thaliana* roots are differently modulated by all the seven dusts, probably because of the peculiar mechanisms of action of the different chemical compounds of each dust.

The alteration of the root cell redox homeostasis, due to dust exposure, causing a variation of NO concentration and localization, was also related to different $O_2\cdot^-$ levels, as shown by NBT assay (Fig. 6).

In the roots not exposed to dusts, NBT staining was very weak in the basal portion of the LRPs, while in the LRs and PRs was strictly localized in the vasculature of the elongation and differentiation zones and absent in the apical meristem (Fig. 6, A-C). Brake dust treatment (Fig. 6, D-F) significantly increased the NBT staining and pattern both in the LRs and PRs and in the LRPs. Indeed, in this treatment the signal was expressed in the entire LRPs, including the surrounding tissues, while was heavily located in the tip and in the vasculature of the LRs and PRs.

Pellet ash treatment (Fig. 6, G-I) greatly delocalized and increased the staining, especially in the meristematic zone of LRs and PRs, while low effects were detected in the LRPs compared to the NIST and BD treatments.

In the LRPs treated with RD, the $O_2\cdot^-$ signal was comparable to the control, while the LRs and PRs showed an increase of the signal in the differentiation and elongation zones, and it was quite extended to the

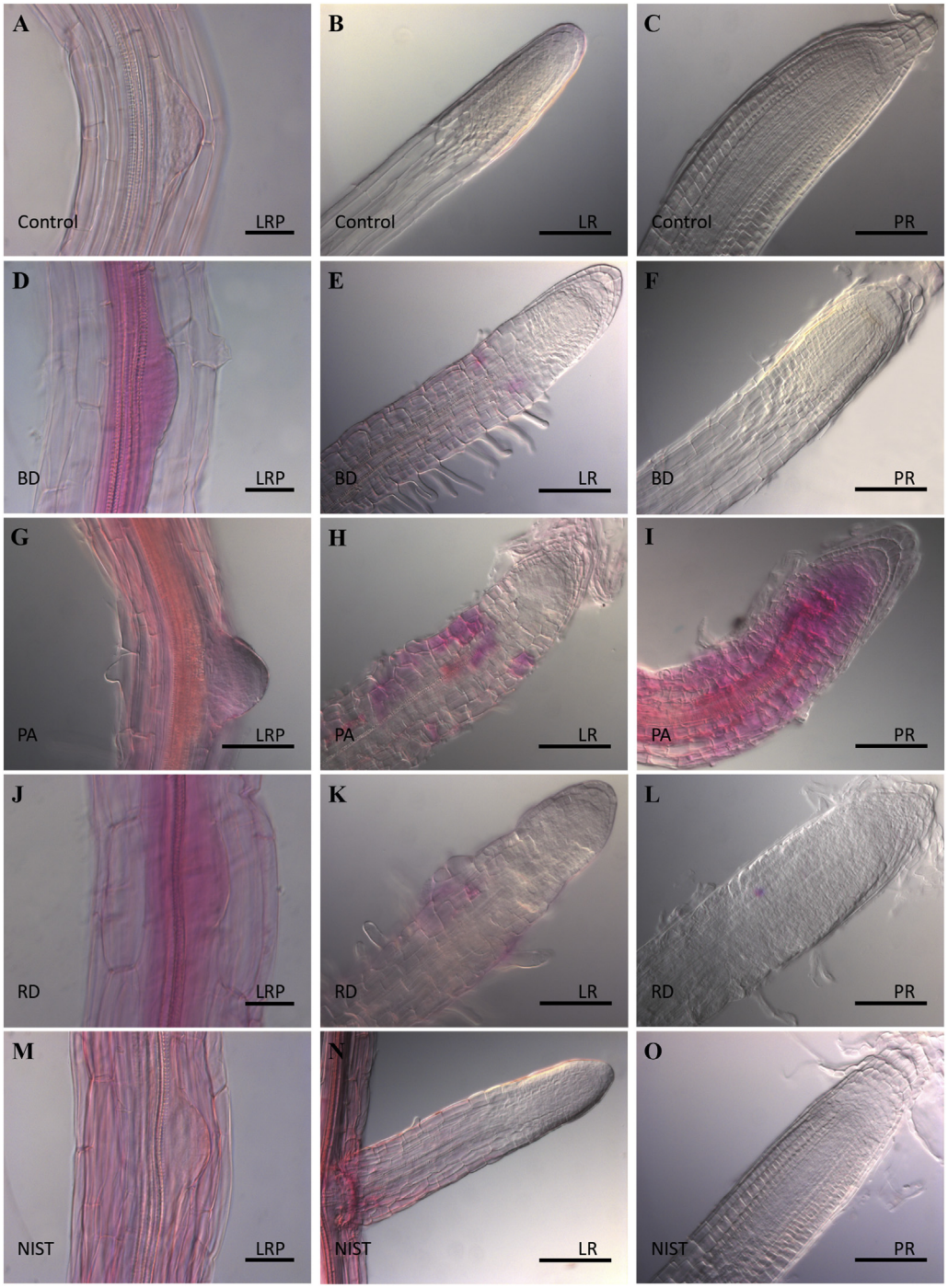

Fig. 7. Lipid peroxidation highlighted by Schiff's reagent in *A. thaliana* LRPs, LRs and PRs not exposed (control, A–C) or exposed to BD (D–F), PA (G–I), RD (J–L) and NIST (M–O). Bars: = 30 μm (A, D, J, M) and 100 μm (B–C; E–I; K–L; N–O).

meristematic zone of the root (Fig. 6, J-L). Finally, NIST (Fig. 6, M-O) treated LRPs showed a strong increase of the staining, which deeply covered the entire LRPs, while in the LRs and PRs spread in a similar manner to BD treatment. These analyses demonstrated that all the examined dusts were able to induce an increase of $O_2\cdot^-$ production in *A. thaliana* roots. In addition, dust-related $O_2\cdot^-$ production involved root tissues where $O_2\cdot^-$ is normally present at very low concentration, such as in the root apical meristem.

The damaging effects of the oxidative stress of the selected dusts, which are related to a variation in both NO and $O_2\cdot^-$ accumulation and localization were also highlighted by the Schiff test in the *A. thaliana* roots. Schiff's reagent reacts with aldehydes that originate from lipid peroxides downstream of reactive oxygen species to produce an imine, also called a Schiff base, which is magenta or purple in color, thus representing a useful tool for the indirect detection of lipid peroxidation (Gilbert and Martin, 2016).

All the examined dusts increased the lipid peroxidation of *A. thaliana* seedling roots, with the strongest effects induced by PA and RD (Fig. 7). Control of LRs and PRs did not show notable dye formation, except for a faint staining in the tissues of PRs next to the forming LRPs and in the epidermis of the same LRPs (Fig. 7A-C). This fact is probably due to the histochemical reaction between the reagent and the by-products of enzymes, whose activity is related to cortical cell separation during the lateral root primordium emergence (Seo et al., 1998). In all

the treatments, histochemical staining in the LRPs significantly increased compared to the control LRPs (Fig. 7D, G, J, M). Moreover, the stele, cortex and epidermis tissues of the PRs mature zone of the roots exposed to PA were positive to Schiff reaction (Fig. 7I). The BD treatment induced a localized staining in the LRPs and in the vascular tissues and pericycle of the PRs close to the LRPs (Fig. 7D). NIST and BD-treated LR tips showed a slight increase of the staining (Fig. 7N,E). Road dust and PA-treated LRs showed a more evident peroxidation process activity with respect to the control (Fig. 7K,H). Pellet ash was the treatment that most affected the *A. thaliana* cell membrane roots integrity. In fact, in this treatment both the LRs and the PRs showed a very strong and widespread histochemical staining, reflecting a deep degradation of the cell membrane lipids. (Fig. 7G-I) The toxicity of PA also affected the definition of the root tissues, causing a precocious differentiation of the primary tissues in LRs (Fig. 7 H). Lastly, *A. thaliana* RD, NIST and BD-treated PR tips did not, or only weakly showed, an increase of the histochemical staining, compared to the control (Fig. 7).

Overall, results showed that BD, PA, RD and NIST can deeply alter the cellular redox homeostasis of *A. thaliana* roots, acting on the biosynthesis and distribution of NO and $O_2\cdot^-$ and thus leading to oxidative damages and root cell membrane degradation. In addition, the generation of superoxide anion and nitric oxide in plant cells may lead to the formation of more reactive oxygen and nitrogen species such as hydroxyl radical (·OH), singlet oxygen ($^1O_2$) and peroxynitrite ($ONOO^-$), each of which may cause membrane lipid peroxidation and cellular damages, as previously reported for *A. thaliana* (Triantaphylidès et al., 2008; Corpas and Barroso, 2014).

The observed increase and distribution alteration of NO and $O_2\cdot^-$ in *A. thaliana* roots may be explained by the high bioaccumulation of toxic elements and heavy metals in the seedlings grown in the presence of the PM-selected components. In addition, this has been confirmed by several reports, which highlighted the role of both NO and $O_2\cdot^-$ as key mediators of metal toxicity in plants (Singh et al., 2017; Yuan and Huang, 2016). It is worth nothing that also the less bioaccumulated elements such as As, Cr and Ni, which can be toxic at very low concentrations, may have contributed to the oxidative damages observed in the *A. thaliana* roots. Pellet ash was the treatment that mostly affected the oxidative balance in the *A. thaliana* roots and the high bioaccumulation of Mn and K in the PA-treated seedlings was probably the main cause of the strong increase of NO and $O_2\cdot^-$ observed in the LRs and PRs.

Finally, Schiff's reagent analyses confirmed the role of the dusts as strong oxidizing agents, which ultimately led to lipid peroxidation and membrane injury in *A. thaliana* roots, by acting on the NO and $O_2\cdot^-$ content and distribution. Here too, PA treated roots were the most stained, revealing a close correspondence between aldehydes accumulation, NO and $O_2\cdot^-$ content in roots, thus indicating PA as the most toxic PM-selected component tested.

The different alteration of the cellular redox homeostasis in the roots of the *A. thaliana* seedlings exposed to the atmospheric dusts confirmed that the divergent relative sensitivity of the AA (more sensitive for BD and NIST), DTT and DCFH (more sensitive for PA) assays toward the PM-selected components is mainly due to the peculiar oxidative mechanisms of actions of their different chemical compounds.

4. Conclusions

We evaluated the oxidative potentials and the effects of 7 PM-selected components, previously chemically analysed, on the model plant *A. thaliana*. Bioaccumulation of the elements of the atmospheric dusts in the *A. thaliana* seedlings was determined and both root morphological and oxidative stress analyses were performed.

Brake dust, PA and NIST showed the highest oxidative potentials. In fact, BD and NIST were the most responsive dusts to the OP^{AA} assay, while PA was the dust with the highest values for OP^{DTT} and OP^{DCFH} assays. Except for S and SD, all the examined dusts altered *A. thaliana* root morphology, with the strongest effects for the dusts that showed the highest OPs (BD, PA and NIST). Indeed, brake dust and pellet ash were the only PM-selected components that inhibited primary root growth, while urban dust heavily inhibited lateral root density. High concentrations of Cs, Li, Nb, Pb, Sb, Sn, Tl, V, W and Zr were found to be accumulated in the tissues of the seedlings exposed to BD; Mn and W in the seedlings grown in the presence of PA and Al, Cd, Pb, Sn, Ti, V, W, Zr in the seedlings exposed to NIST. PCA revealed correlations among OPs of the dusts, element bioaccumulation and root morphology alteration, identifying the most responsible dust-associated elements affecting the plant model organism. OP^{DTT} and OP^{DCFH} were found to be well correlated with the K and Mn concentrations accumulated in the *A. thaliana* seedlings exposed to PA, while OP^{AA} appeared to be related with Mo and other elements bioaccumulated in BD, RD and NIST samples. Moreover, OPs of the dusts were found to be positively correlated with PRL and LRD inhibition. Therefore, BD, PA and NIST were identified as the PM-selected components with the highest potential inducing oxidative stress and root development alteration.

The analysis of $O_2\cdot^-$ and NO production and cell membrane oxidation in *A. thaliana* roots confirmed the capacity of the dusts to induce oxidative stress, leading to plant redox homeostasis alteration and root cellular damages, and verified the reliability of the OP assays for the prediction of the ROS and RNS generation pathways in biological organisms. Indeed, the highest levels of NO and O^{-2} and lipid peroxidation in *A. thaliana* roots were observed after the treatment with PA, BD and NIST which, as previously mentioned, were the dusts with the highest OPs.

Finally, our study validated *A. thaliana* as a suitable model for bioindicator studies and encourage its employment for further investigations about the detection of PM toxicity on living organisms.

Acknowledgments

This work was partially funded by the project 2017 RG11715C7C8801CF (Principal Investigator Dr. S. Canepari), financed by Sapienza University of Rome.

The authors gratefully thank Valeria Vicarietti for her help in the morphological and chemical analyses of the samples and Martina Ristorini and Maria Agostina Frezzini for their support in the application of the oxidative potential assays on the examined atmospheric dusts.

Author contributions

L. Massimi, D. Piacentini, S. Canepari and G. Falasca conceived and planned the experiments; L. Massimi performed the oxidative potential, chemical and multivariate statistical analyses; D. Piacentini performed the morphological and oxidative stress analyses; L. Massimi and D. Piacentini elaborated the data and wrote the manuscript; S. Canepari and G. Falasca coordinated the group and supervised the manuscript.

Declaration of competing interest

The authors declare that they have no known competing financial interests or personal relationships that could have appeared to influence the work reported in this paper.

Appendix A. Supplementary data

Supplementary data to this article can be found online at https://doi.org/10.1016/j.envint.2019.105094.

References

Abdoli, M.A., Golzary, A., Hosseini, A., Sadeghi, P., 2018. Wood pellet emissions. In:

Wood Pellet as a Renewable Source of Energy. Springer International Publishing, Cham, pp. 161–184. https://doi.org/10.1007/978-3-319-74482-7.
Achary, V.M.M., Jena, S., Panda, K.K., Panda, B.B., 2008. Aluminium induced oxidative stress and DNA damage in root cells of Allium cepa L. Ecotoxicol. Environ. Saf. 70 (2), 300–310.
Astolfi, M.L., Marconi, E., Protano, C., Vitali, M., Schiavi, E., Mastromarino, P., Canepari, S., 2018. Optimization and validation of a fast digestion method for the determination of major and trace elements in breast milk by ICP-MS. Anal. Chim. Acta 1040, 49–62.
Bates, J.T., Fang, T., Verma, V., Zeng, L., Weber, R.J., Tolbert, P.E., Abrams, J.Y., Sarnat, S.E., Klein, M., Mulholland, J.A., Russell, A.G., 2019. Review of acellular assays of ambient particulate matter oxidative potential: methods and relationships with composition, sources, and health effects. J. Environ. Sci. Technol. 53 (8), 4003–4019.
Brook, R.D., Rajagopalan, S., Pope 3rd, C.A., Brook, J.R., Bhatnagar, A., Diez-Roux, A.V., Holguin, F., Hong, Y., Luepker, R.V., Mittleman, M.A., Peters, A., Siscovick, D., Smith Jr., S.C., Whitsel, L., Kaufman, J.D., 2010. Particulate matter air pollution and cardiovascular disease: an update to the scientific statement from the American Heart Association. Circulation 121 (21), 2331–2378.
Cachon, B.F., Firmin, S., Verdin, A., Ayi-Fanou, L., Billet, S., Cazier, F., Martin, P.J., Aissi, F., Courcot, D., Sanni, A., Shirali, P., 2014. Proinflammatory effects and oxidative stress within human bronchial epithelial cells exposed to atmospheric particulate matter (PM2. 5 and PM > 2.5) collected from Cotonou, Benin. Environ. Pollut. 185, 340–351.
Canepari, S., Cardarelli, E., Giuliano, A., Pietrodangelo, A., 2006a. Determination of metals, metalloids and non-volatile ions in airborne particulate matter by a new two-step sequential leaching procedure part a: experimental design and optimization. Talanta 69 (3), 581–587.
Canepari, S., Cardarelli, E., Pietrodangelo, A., Strincone, M., 2006b. Determination of metals, metalloids and non-volatile ions in airborne particulate matter by a new two-step sequential leaching procedure: part B: validation on equivalent real samples. Talanta 69 (3), 588–595.
Canepari, S., Perrino, C., Olivieri, F., Astolfi, M.L., 2008. Characterisation of the traffic sources of PM through size-segregated sampling, sequential leaching and ICP analysis. Atmos. Environ. 42 (35), 8161–8175.
Canepari, S., Pietrodangelo, A., Perrino, C., Astolfi, M.L., Marzo, M.L., 2009. Enhancement of source traceability of atmospheric PM by elemental chemical fractionation. Atmos. Environ. 43 (31), 4754–4765.
Canepari, S., Marconi, E., Astolfi, M.L., Perrino, C., 2010a. Relevance of Sb (III), Sb (V), and Sb-containing nano-particles in urban atmospheric particulate matter. Anal. Bioanal. Chem. 397 (6), 2533–2542.
Canepari, S., Astolfi, M.L., Moretti, S., Curini, R., 2010b. Comparison of extracting solutions for elemental fractionation in airborne particulate matter. Talanta 82 (2), 834–844.
Charrier, J.G., Anastasio, C., 2012. On dithiothreitol (DTT) as a measure of oxidative potential for ambient particles: evidence for the importance of soluble transition metals. Atmos. Chem. Phys. 12 (5), 11317.
Chirizzi, D., Cesari, D., Guascito, M.R., Dinoi, A., Giotta, L., Donateo, A., Contini, D., 2017. Influence of Saharan dust outbreaks and carbon content on oxidative potential of water-soluble fractions of PM2. 5 and PM10. Atmos. Environ. 163, 1–8.
Conti, M.E., Iacobucci, M., Cucina, D., Mecozzi, M., 2007. Multivariate statistical methods applied to biomonitoring studies. Int. J. Environ. Pollut. 29 (1–3), 333–343.
Corpas, F.J., Barroso, J.B., 2014. Peroxynitrite ($ONOO^-$) is endogenously produced in Arabidopsis peroxisomes and is overproduced under cadmium stress. Ann. Bot. 113 (1), 87–96.
Costabile, F., Gualtieri, M., Canepari, S., Tranfo, G., Consales, C., Grollino, M.G., Paci, E., Petralia, E., Pigini, D., Simonetti, G., 2019. Evidence of association between aerosol properties and in-vitro cellular oxidative response to PM1, oxidative potential of PM2.5, a biomarker of RNA oxidation, and its dependency on the combustion aerosol. Atmos. Environ. 213, 444–455.
Councell, T.B., Duckenfield, K.U., Landa, E.R., Callender, E., 2004. Tire-wear particles as a source of zinc to the environment. J. Environ. Sci. Technol. 38 (15), 4206–4214.
Daresta, B.E., Italiano, F., de Gennaro, G., Trotta, M., Tutino, M., Veronico, P., 2015. Atmospheric particulate matter (PM) effect on the growth of Solanum lycopersicum cv. Roma plants. Chemosphere 119, 37–42.
Della Rovere, F., Fattorini, L., D'Angeli, S., Veloccia, A., Falasca, G., Altamura, M.M., 2013. Auxin and cytokinin control formation of the quiescent Centre in the adventitious root apex of Arabidopsis. Ann. Bot. 112 (7), 1395–1407.
Di Dato, C., Gianfrilli, D., Greco, E., Astolfi, M., Canepari, S., Lenzi, A., Isidori, A.M., Giannetta, E., 2017. Profiling of selenium absorption and accumulation in healthy subjects after prolonged L-selenomethionine supplementation. J. Endocrinol. Investig. 40 (11), 1183–1190.
Dodd, M.D., Ebbs, S.D., Gibson, D.J., Filip, P., 2014. Alteration of root growth by lettuce, wheat, and soybean in response to wear debris from automotive brake pads. Arch. Environ. Contam. Toxicol. 67 (4), 557–564.
Evans, J., van Donkelaar, A., Martin, R.V., Burnett, R., Rainham, D.G., Birkett, N.J., Krewski, D., 2013. Estimates of global mortality attributable to particulate air pollution using satellite imagery. Environ. Res. 120, 33–42.
Fattorini, L., Ronzan, M., Piacentini, D., Della Rovere, F., De Virgilio, C., Sofo, A., Altamura, M.M., Falasca, G., 2017. Cadmium and arsenic affect quiescent Centre formation and maintenance in Arabidopsis thaliana post-embryonic roots disrupting auxin biosynthesis and transport. Environ. Exp. Bot. 144, 37–48.
Feigl, G., Lehotai, N., Molnár, Á., Ördög, A., Rodríguez-Ruiz, M., Palma, J.M., Corpas, F.J., Erdei, L., Kolbert, Z., 2014. Zinc induces distinct changes in the metabolism of reactive oxygen and nitrogen species (ROS and RNS) in the roots of two Brassica species with different sensitivity to zinc stress. Ann. Bot. 116 (4), 613–625.
Gilardoni, S., Massoli, P., Paglione, M., Giulianelli, L., Carbone, C., Rinaldi, M., Decesari, S., Sandrini, S., Costabile, F., Gobbi, G.P., Pietrogrande, M.C., Visentin, M., Scotto, F., Fuzzi, S., Facchini, M.C., 2016. Direct observation of aqueous secondary organic aerosol from biomass-burning emissions. Proc. Natl. Acad. Sci. 113 (36), 10013–10018.
Gilbert, J.C., Martin, S.F., 2016. Experimental organic chemistry: a miniscale & microscale approach, sixth ed. Cengage Learning, CA.
Kelly, F.J., Fussell, J.C., 2012. Size, source and chemical composition as determinants of toxicity attributable to ambient particulate matter. Atmos. Environ. 60, 504–526.
Knaapen, A.M., Borm, P.J., Albrecht, C., Schins, R.P., 2004. Inhaled particles and lung cancer. Part a: mechanisms. Int. J. Cancer 109 (6), 799–809.
Li, R., Kou, X., Geng, H., Xie, J., Yang, Z., Zhang, Y., Cai, Z., Dong, C., 2015. Effect of ambient PM 2.5 on lung mitochondrial damage and fusion/fission gene expression in rats. Chem. Res. Toxicol. 28, 408–418.
Liu, M., Liu, X.X., He, X.L., Liu, L.J., Wu, H., Tang, C.X., Zhang, Y.S., Jin, C.W., 2017. Ethylene and nitric oxide interact to regulate the magnesium deficiency-induced root hair development in Arabidopsis. New Phytol. 213 (3), 1242–1256.
Maiorana, S., Teoldi, F., Silvani, S., Mancini, A., Sanguineti, A., Mariani, F., Cella, C., Lopez, A., Potenza, M.A.C., Lodi, M., Dupin, D., Sanvito, T., Bonfanti, A., Benfenati, E., Baderna, D., 2019. Phytotoxicity of wear debris from traditional and innovative brake pads. Environ. Int. 123, 156–163.
Marcoccia, M., Ronci, L., De Matthaeis, E., Setini, A., Perrino, C., Canepari, S., 2017. In-vivo assesment of the genotoxic and oxidative stress effects of particulate matter on Echinogammarus veneris. Chemosphere 173, 124–134.
Massimi, L., Ristorini, M., Eusebio, M., Florendo, D., Adeyemo, A., Brugnoli, D., Canepari, S., 2017. Monitoring and evaluation of Terni (Central Italy) air quality through spatially resolved analyses. Atmosphere 8 (10), 200.
Massimi, L., Giuliano, A., Astolfi, M.L., Congedo, R., Masotti, A., Canepari, S., 2018. Efficiency evaluation of food waste materials for the removal of metals and metalloids from complex multi-element solutions. Materials 11 (3), 334.
Massimi, L., Conti, M.E., Mele, G., Ristorini, M., Astolfi, M.L., Canepari, S., 2019. Lichen transplants as indicators of atmospheric element concentrations: a high spatial resolution comparison with PM10 samples in a polluted area (Central Italy). Ecol. Indic. 101, 759–769.
Murashige, T., Skoog, F., 1962. A revised medium for rapid growth and bio assays with tobacco tissue cultures. Physiol. Plant. 15 (3), 473–497.
Nel, A., 2005. Air pollution-related illness: effects of particles. Science 308 (5723), 804–806.
de Oliveira Alves, N., Loureiro, A.L.M., Dos Santos, F.C., Nascimento, K.H., Dallacort, R., de Castro Vasconcellos, P., de Souza Hacon, S., Artaxo, P., De Medeiros, S.R.B., 2011. Genotoxicity and composition of particulate matter from biomass burning in the eastern Brazilian Amazon region. Ecotoxicol. Environ. Saf. 74 (5), 1427–1433.
Pant, P., Harrison, R.M., 2013. Estimation of the contribution of road traffic emissions to particulate matter concentrations from field measurements: a review. Atmos. Environ. 77, 78–97.
Perrino, C., Catrambone, M., Farao, C., Canepari, S., 2016. Assessing the contribution of water to the mass closure of PM10. Atmos. Environ. 140, 555–564.
Perrone, M.G., Zhou, J., Malandrino, M., Sangiorgi, G., Rizzi, C., Ferrero, L., Dommen, J., Bolzacchini, E., 2016. PM chemical composition and oxidative potential of the soluble fraction of particles at two sites in the urban area of Milan, northern Italy. Atmos. Environ. 128, 104–113.
Popek, R., Przybysz, A., Gawrońska, H., Klamkowski, K., Gawroński, S.W., 2018. Impact of particulate matter accumulation on the photosynthetic apparatus of roadside woody plants growing in the urban conditions. Ecotoxicol. Environ. Saf. 163, 56–62.
Reche, C., Viana, M., Amato, F., Alastuey, A., Moreno, T., Hillamo, R., Teinilä, K., Saarnio, K., Seco, R., Peñuelas, J., Mohr, C., Prévôt, A.S., Querol, X., 2012. Biomass burning contributions to urban aerosols in a coastal Mediterranean City. Sci. Total Environ. 427, 175–190.
Ronzan, M., Piacentini, D., Fattorini, L., Della Rovere, F., Eiche, E., Riemann, M., Altamura, M.M., Falasca, G., 2018. Cadmium and arsenic affect root development in Oryza sativa L. negatively interacting with auxin. Environ. Exp. Bot. 151, 64–75.
Seo, M., Akaba, S., Oritani, T., Delarue, M., Bellini, C., Caboche, M., Koshiba, T., 1998. Higher activity of an aldehyde oxidase in the auxin-overproducing superroot1 mutant of Arabidopsis thaliana. Plant Physiol. 116 (2), 687–693.
Sharma, P., Jha, A.B., Dubey, R.S., Pessarakli, M., 2012. Reactive oxygen species, oxidative damage, and antioxidative defense mechanism in plants under stressful conditions. J. Bot. 2012, 1–26. https://doi.org/10.1155/2012/217037.
Shi, T., Knaapen, A.M., Begerow, J., Birmili, W., Borm, P.J.A., Schins, R.P.F., 2003a. Temporal variation of hydroxyl radical generation and 8-hydroxy-2′-deoxyguanosine formation by coarse and fine particulate matter. Occup. Environ. Med. 60 (5), 315–321.
Shi, T., Schins, R.P., Knaapen, A.M., Kuhlbusch, T., Pitz, M., Heinrich, J., Borm, P.J., 2003b. Hydroxyl radical generation by electron paramagnetic resonance as a new method to monitor ambient particulate matter composition. J. Environ. Monit. 5 (4), 550–556.
Simonetti, G., Conte, E., Massimi, L., Frasca, D., Perrino, C., Canepari, S., 2018a. Oxidative potential of particulate matter components generated by specific emission sources. J. Aeros. Scien. 126, 99–109.
Simonetti, G., Conte, E., Perrino, C., Canepari, S., 2018b. Oxidative potential of size-segregated PM in an urban and an industrial area of Italy. Atmos. Environ. 187, 292–300.
Singh, H.P., Batish, D.R., Kohli, R.K., Arora, K., 2007. Arsenic-induced root growth inhibition in mung bean (Phaseolus aureus Roxb.) is due to oxidative stress resulting from enhanced lipid peroxidation. Plant Growth Regul. 53 (1), 65–73.
Singh, P.K., Indoliya, Y., Chauhan, A.S., Singh, S.P., Singh, A.P., Dwivedi, S., Tripathi, R.D., Chakrabarty, D., 2017. Nitric oxide mediated transcriptional modulation enhances plant adaptive responses to arsenic stress. Sci. Rep. 7 (1), 3592.

Sofo, A., Vitti, A., Nuzzaci, M., Tataranni, G., Scopa, A., Vangronsveld, J., Remans, T., Falasca, G., Altamura, M.M., Degola, F., Sanità di Toppi, L., 2013. Correlation between hormonal homeostasis and morphogenic responses in Arabidopsis thaliana seedlings growing in a cd/cu/Zn multi-pollution context. Physiol. Plant. 149 (4), 487–498.

Taioli, E., Sram, R.J., Garte, S., Kalina, I., Popov, T.A., Farmer, P.B., 2007. Effects of polycyclic aromatic hydrocarbons (PAHs) in environmental pollution on exogenous and oxidative DNA damage (EXPAH project): description of the population under study. Mutat. Res. 620 (1), 1–6.

Thorpe, A., Harrison, R.M., 2008. Sources and properties of non-exhaust particulate matter from road traffic: a review. Sci. Total Environ. 400 (1–3), 270–282.

Toscano, G., Duca, D., Amato, A., Pizzi, A., 2014. Emission from realistic utilization of wood pellet stove. Energy 68, 644–650.

Triantaphylidès, C., Krischke, M., Hoeberichts, F.A., Ksas, B., Gresser, G., Havaux, M., Van Breusegem, F., Mueller, M.J., 2008. Singlet oxygen is the major reactive oxygen species involved in photooxidative damage to plants. Plant Physiol. 148 (2), 960–968.

Trifuoggi, M., Pagano, G., Oral, R., Gravina, M., Toscanesi, M., Mozzillo, M., Siciliano, A., Burić, P., Lyons, D.M., Palumbo, A., Thomas, P.J., D'Ambra, L., Crisci, A., Guida, M., Tommasi, F., 2019. Topsoil and urban dust pollution and toxicity in Taranto (southern Italy) industrial area and in a residential district. Environ. Monit. Assess. 191 (1), 43. https://doi.org/10.1007/s10661-018-7164-7.

Van Norman, J.M., Benfey, P.N., 2009. Arabidopsis thaliana as a model organism in systems biology. Wiley Interdiscip. Rev. Syst. Biol. Med. 1 (3), 372–379.

Verma, A., Singh, S.N., 2006. Biochemical and ultrastructural changes in plant foliage exposed to auto-pollution. Environ. Monit. Assess. 120 (1–3), 585–602.

Vernile, P., Tutino, M., Bari, G., Amodio, M., Spagnuolo, M., de Gennaro, G., de Lillo, E., 2013. Particulate matter toxicity evaluation using bioindicators and comet assay. Aerosol Air Qual. Res. 13, 172–178.

Vitti, A., Nuzzaci, M., Scopa, A., Tataranni, G., Tamburrino, I., Sofo, A., 2014. Hormonal response and root architecture in Arabidopsis thaliana subjected to heavy metals. Int. J. Plant Biol. 5 (1), 16–21.

Weigel, D., Glazebrook, J., 2002. Arabidopsis: A Laboratory Manual, first ed. CSHL Press, New York.

Wong-Ekkabut, J., Xu, Z., Triampo, W., Tang, I.M., Tieleman, D.P., Monticelli, L., 2007. Effect of lipid peroxidation on the properties of lipid bilayers: a molecular dynamics study. Biophys. J. 93 (12), 4225–4236.

Xiong, Q., Yu, H., Wang, R., Wei, J., Verma, V., 2017. Rethinking dithiothreitol-based particulate matter oxidative potential: measuring dithiothreitol consumption versus reactive oxygen species generation. Environ. Sci. Technol. 51 (11), 6507–6514.

Yamamoto, Y., Kobayashi, Y., Devi, S.R., Rikiishi, S., Matsumoto, H., 2003. Oxidative stress triggered by aluminum in plant roots. Plant Soil 255 (1), 239–243.

Yuan, H.M., Huang, X., 2016. Inhibition of root meristem growth by cadmium involves nitric oxide-mediated repression of auxin accumulation and signalling in Arabidopsis. Plant Cell Environ. 39 (1), 120–135.

Zanella, L., Fattorini, L., Brunetti, P., Roccotiello, E., Cornara, L., D'Angeli, S., Della Rovere, F., Cardarelli, M., Barbieri, M., Sanità di Toppi, L., Degola, F., Lindberg, S., Altamura, M.M., Falasca, G., 2016. Overexpression of AtPCS1 in tobacco increases arsenic and arsenic plus cadmium accumulation and detoxification. Planta 243 (3), 605–622.

Zhao, J., Wang, W., Zhou, H., Wang, R., Zhang, P., Wang, H., Pan, X., Xu, J., 2017. Manganese toxicity inhibited root growth by disrupting auxin biosynthesis and transport in Arabidopsis. Front. Plant Sci. 8, 272. https://doi.org/10.3389/fpls.2017.00272.

Zou, Y., Jin, C., Su, Y., Li, J., Zhu, B., 2016. Water soluble and insoluble components of urban PM2. 5 and their cytotoxic effects on epithelial cells (A549) in vitro. Environ. Pollut. 212, 627–635.